A Crucial Wave Detection and Delineation Method for Twelve-Lead ECG Signals

GENLANG CHEN[1,2], **MAOLIN CHEN**[3], **JIAJIAN ZHANG**[3], **LIANG ZHANG**[4], **AND CHAOYI PANG**[1,2]

[1]Ningbo Institute of Technology, Zhejiang University, Ningbo 315100, China
[2]Ningbo Research Institute, Zhejiang University, Ningbo 315100, China
[3]College of Computer Science and Technology, Zhejiang University, Hangzhou 310021, China
[4]Ningbo Municipal Center for Disease Control and Prevention, Ningbo 315100, China

Corresponding authors: Genlang Chen (cgl@zju.edu.cn) and Liang Zhang (zhangl@nbcdc.org.cn)

ABSTRACT Delineating the crucial waves in electrocardiogram records is a paramount work for the automatic diagnosis system of heart diseases. In this paper, a novel method is described to determine the boundaries and the peaks of P waves, QRS complexes and T waves by utilizing twelve-lead electrocardiogram signals. It avoids the difficulty of setting the thresholds when determining the boundaries of crucial waves and also the trouble of selection of wavelet basis as the wavelet-based method does. The signals are first preprocessed by a bandpass filter. After that, the locations of QRS complexes are identified. And based on the QRS locations, adaptive search windows are set to detect the locations of P waves and T waves. Then, a method called local distance transform decides the wave boundary in each lead. Finally, the final boundary determination rule is applied to obtain reliable boundaries. We justify the performance of our algorithm on LUDB database. When the tolerance window interval is 40ms, the peak accuracies of P wave, QRS complex and T wave are all beyond 98% and their boundary accuracies are all above 96%. Compared with the derivative threshold method and the wavelet-based method where the tolerance window interval is 150ms, the algorithm shows a sensitivity and a positive predictive value of peaks and boundaries greater than or equal to 98.43% and 96.44% for the P wave, 99.89% and 99.86% for the QRS complex and 99.21% and 99.85% for the T wave. For the critera of average error and standard deviation, our method has the performance similar to those methods. In addition, our algorithm can also handle such several situations where the boundary determination of crucial waves is tough as high T wave, high noise and baseline wandering well.

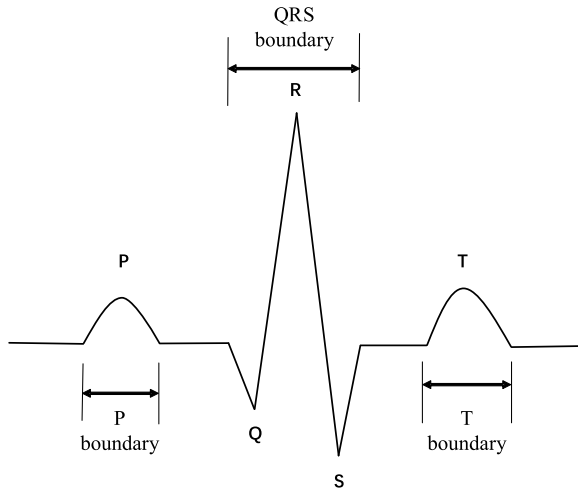**INDEX TERMS** ECG, twelve-lead signals, local distance transform, detection, delineation.

I. INTRODUCTION

Early detection of cardiac abnormalities becomes extremely important with the increasing number of people who die of heart diseases every year. Electrocardiogram (ECG) as an effective non-invasive tool to record the health state of the heart presents heart electrical activities in a graphic form. In the clinical environment, physicians analyze the ECG records of patients to judge whether they have a benign or unkind heart state. Yet the analysis process is pretty much laborious and repetitive. In the past several decades, many researchers focused on the automatic diagnosis of cardiovascular diseases to reduce the labor cost of analyzing ECG.

Usually, an automatic ECG diagnosis system includes such several procedures as preprocessing, feature extraction, feature selection, feature transform, and disease classification. In reality, ECG signal is easily contaminated by different kinds of noises, namely electrode contact noise, powerline interference, baseline wander, electrode motion artifact, electrocardiography artifact, muscle artifacts, equipment noise and quantization noise [1]. A preprocessing step must be practiced to exclude them. Next, the automatic diagnosis system needs to delineate ECG signal, that is, to identify the peak and boundary of P wave, QRS complex, and T wave in each beat of ECG signal, as shown in Fig. 1. As a

The associate editor coordinating the review of this manuscript and approving it for publication was Chao Shen.

FIGURE 1. The feature points of normal ECG.

fundamental work, it provides abundant morphological, interval and amplitude features for the following cardiovascular disease classification and even enhances the interpretability of the automatic diagnosis system. Thus this step is paramount in these procedures.

In literature, many researchers have worked on the delineation of ECG signal. Pan and Tompkins [2] proposed a distinguished algorithm for real-time QRS complex detection based on differentiating, squaring and integrating operation, which can effectively detect the QRS complex locations and delineate QRS complex boundaries. Laguna *et al.* [3] utilized the first derivative and wave morphology to detect the QRS complex and T wave. Laguna *et al.* [4] presented a twelve-lead automatically delineating algorithm, using derivative threshold and taking all leads into account for deciding the characteristic wave boundaries. The authors [5]–[8] detected the characteristic points in ECG signal by wavelet transform and obtained an acceptable performance. Afonso *et al.* [9] designed a multi-rate digital signal processing algorithm by using filter banks to detect the QRS complex. Sun *et al.* [10] proposed a multiscale morphological derivative (MMD) transform-based singularity detector to detect the fiducial points of P wave, QRS complex, and T wave. Andreao *et al.* [11] showed an original hidden Markov model approach for the purpose of online beat segmentation and classification of electrocardiograms, which addressed a series of problems like waveform modeling, multichannel beat segmentation and classification. The authors [12] used adaptive piecewise constant approximation (APCA) and piecewise derivative dynamic time warping (PDDTW) to segment a single lead ECG signal.

In other papers, researchers also employed machine learning methods on the delineation of ECG signal. The authors [13], [14] trained a support vector machine (SVM) classifier for the detection and delineation of P wave and T wave. Saini *et al.* [15] used the k-nearest neighbors (KNN) model for locating P wave and T wave and deciding their boundaries.

Besides these, researchers also applied a totally adaptive signal processing technique called empirical mode decomposition (EMD) which is often used for nonlinear, nonstationary time series signals to extract the fiducial point information of ECG signal. The method decomposes time series signal into multiple intrinsic mode functions (IMFs), which meet the sum of those functions is equal to the original signal. The authors [16] suppressed baseline wander and high-frequency noise by removing selective high order IMFs and low order IMFs and then detected QRS complex following a nonlinear transformation. It validly increased the detection accuracy of QRS complex. The authors [17] combined adaptive thresholding technique and EMD algorithm to delineate the QRS complex. Rezgui and Lachiri [18] verified the effectiveness of ensemble empirical mode decomposition, a variant of EMD, in the detection of wave peaks.

Recently, Ning and Selesnick [19] detected QRS complex after ECG enhancement based on sparse derivatives and obtained a promising result. Bayasi *et al.* [20] developed a novel robust and adaptive P wave and T wave delineation method depending on ECG signal filtering, backward and forward search windows and adaptive thresholds. The authors [21] introduced a sequential Bayesian method to simultaneously detect and delineate P wave and T wave as well as estimate their waveform on a beat-to-beat basis. The authors [22] combined particle swarm optimization (PSO) and extended Kalman filter (EKF) to delineate P wave and T wave in an ECG signal. Shaik *et al.* [23] identified and delineated QRS complex, using chirplet transform. The authors [24] segmented the ECG signal to extract P wave, QRS complex and T wave features and track subtle variations of those waves using adaptive Hermite functions. Lee *et al.* [25] utilized polygonal approximation to represent ECG signal as few vertices with a curvature-based vertex selection technique and consequently boosted the accuracy of fiducial point detection.

Most algorithms mentioned above can achieve a desirable result when low noise exist but once the noise becomes too loud, their performance, especially the performance of wave boundary delineation will drop. Meanwhile, most of them were developed in standard databases including MIT-BIH Arrhythmia Database [26], European ST-T Database [27], QT Database [28] and CSE Database [29] which hold few lead ECG signals and lack exhaustive annotations except CSE database. Therefore, it is necessary to develop a robust delineation algorithm that can tolerate some certain noise in a database with twelve-lead signals and thorough annotations. LUDB [30] is such a database. It contains 200 records from 200 individuals and all those records are twelve-lead signals whose duration is 10 seconds. The signals are digitized at 500 samples per second and have intensive annotation about the boundaries and peaks of P wave, QRS complex, and T wave decided by cardiologists.

In this paper, we propose a new algorithm based the LUDB database for delineating characteristic points of ECG waves by considering twelve-lead ECG signals. It avoids
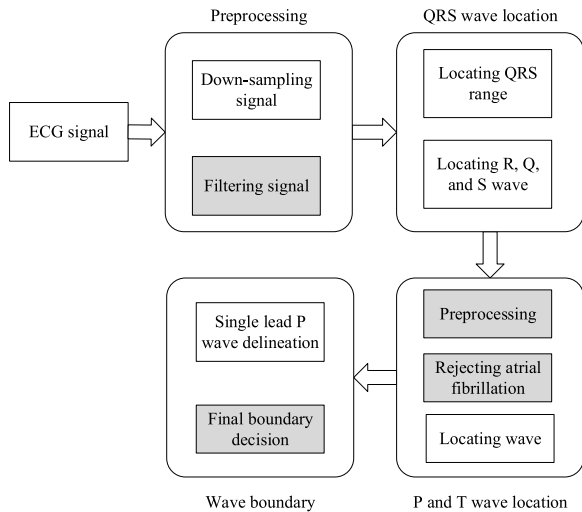
FIGURE 2. The process of the characteristic points detection of twelve-lead ECG signals.

the difficulty of setting the thresholds when determining the boundaries of crucial waves as the derivative threshold method does and also eliminates the trouble of selection of wavelet basis as the wavelet-based method does. This paper is organized as follows. In section II, the algorithm overview first is described and then the details of each procedures are introduced. In section III, the algorithm is evaluated on the LUDB database and is compared with other works. Finally, section IV summarizes our work.

II. METHOD

The overall process about how to detect characteristic points of twelve-lead ECG signals is presented as Fig. 2. First, we down-sample these signals to 200 samples per second and then filter them by a bandpass filter to improve the quality of the signals. Then, we locate the QRS range and recognize the feature points of QRS complex that include the peaks of Q wave, R wave and S wave. Among them, R wave is the most important and stable wave. Its peak is considered as the peak of QRS complex. P wave is detected in an adaptive search window signal before QRS and T wave is recognized by an adaptive window signal behind QRS. Finally, the boundaries of these crucial waves are determined.

In the method, four modules (the shaded areas) are used to improve its robustness. Among them, the filtering signal module and the preprocessing module improve the signal quality. The rejecting atrial fibrillation module discards the atrial fibrillation signals. Additionally, to ensure the reliability of the method further, the twelve-lead boundary annotations are considered to eliminate the false boundary annotations in the final boundary determination module. Ultimately, this proposed method can avoid the difficulty of setting the thresholds when deciding the wave boundaries as the derivative threshold method does and also eliminate the inconvenience of selection of wavelet basis as the wavelet-based method does. The algorithm is described in detail below.
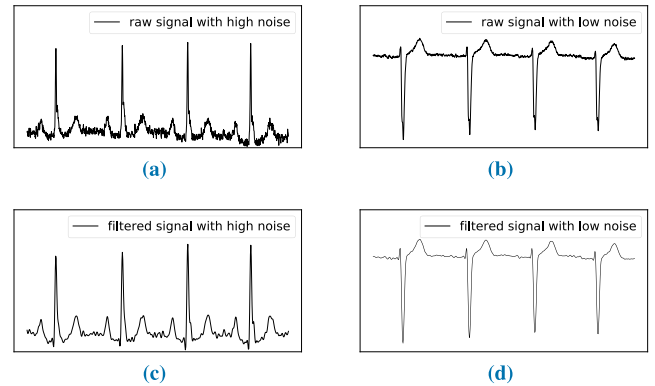
FIGURE 3. Down-sampling and filtering signal. Signal in (a) has high noise and signal in (b) has low noise. Subplots below them display the signals which are down-sampled and filtered.

A. PREPROCESSING

Signal preprocessing is an essential step due to the existence of noise in ECG signal. In LUDB database, the sampling frequency of ECG signal is 500 Hz per second. In this paper, the signal was first down-sampled to 200 samples per second to reduce the processing time and suppress noise to a certain degree. Further, the down-sampled signal passed through the Butterworth bandpass filter which has a frequency response as flat as possible in the given passband. QRS complex has a primary spectrum bandwidth of 0Hz to 38Hz and P wave and T wave have a primary spectrum bandwidth less than 20Hz [31]. We set the bandwidth of our Butterworth bandpass filter to [0.05, 30] Hz. Fig. 3 shows the result of the two procedures. We can find that for the high noisy signal, most of the noise is eliminated and for low noisy ECG signal, the waveform of each primary wave still remains undistorted.

B. QRS LOCATION

1) LOCATING QRS RANGE

In locating QRS complexes, PAN's QRS detection algorithm [2] was chosen which differentiates ECG signal with formula 1, squares the differentiated signal with formula 2 and then integrates the squared signal with formula 3 by a moving window to decide the ranges of QRS complexes in ECG signal. There $Diff(x)$ means the differentiation value of location x in the ECG signal, $Square(x)$ means the square value of location x in the differentiated signal and $Inter$ means the integral value of location x in the squared signal. T is the sampling period and K means the number of signal points during the moving window of the point x. The x_{-i} and x_i presents the value of the next i point in x left side and right side respectively.

$$Diff(x) = \frac{2*x_1 - 2*x_{-1} + x_2 - x_{-2}}{8T} \quad (1)$$

$$Square(x) = x * x \quad (2)$$

$$Inter(x) = \frac{x_{-(k-1)} + \ldots + x_{-1} + x}{k} \quad (3)$$

In the method, we set the moving window size to 90ms. According to the QRS detection algorithm, the rising segment

of integrated signal marks the ranges of QRS complexes in ECG signal. Thus, the integrated signals are differentiated again to get the rising segment ranges for twelve-lead signals by differentiation formula 1.

To improve the reliability of detected QRS complexes, instead of using search back method to preclude false QRS complex ranges which actually are T waves as described in PAN's algorithm, an alternative algorithm is proposed to ensure the reliability of twelve-lead QRS ranges. We agree that $qrs_{i,j}$ represents the jth QRS range in lead i and qrs_k represents the all QRS ranges in lead k. The whole algorithm can be described as Algorithm 1. It first takes QRS ranges of other leads into account and judges whether a given QRS range $qrs_{i,j}$ intersects a certain number of other ranges *intersection_number* in other leads. There, "intersect" means that two QRS ranges overlapped with each other in the time region. If the *intersection_number* is less than the minimal intersection number threshold *min_intersection_number*, the $qrs_{i,j}$ is considered as a wrong range and it is excluded. As a rule, the lager the value of *min_intersection_number* is, the more reliable the detected QRS ranges are. In this paper, the value of *min_intersection_number* is set to eight. In clinical environment, because the distance between adjacent QRS waves has a miminal value *min_distance* (usually greater than 300ms), the algorithm also calculates the distance between $qrs_{i,j}$ and its immediate prior QRS range $qrs_{i,j-1}$ in the same lead to further eliminate false QRS complex ranges. In this paper, if the distance between them is less than 300ms, the range is ignored. Finally, a reliable qrs range should meet these two conditions at the same time.

An example of QRS detection in the LUDB database is showed as Fig. 4. In the figure, consecutive two bold lines represent a preliminary QRS range. The *intersection_number* of the third QRS range in III is four which intersects with the third QRS ranges in aVL, aVF, V2, and V3. It is an error QRS range. Besides this, the distance between the third range in III and its prior QRS range is less than 300ms. According to this, it also should be disregarded. So do the third range in aVL, aVF, V2, and V3.

2) LOCATING R, Q, AND S WAVE

In the following sections, *ECGDer* stands for the derivative signal of a wave, a beat, a lead or even twelve-lead signals. Its calculation formula is the same as formula 1, and the specific meaning depends on the context. The normal QRS complex consists of Q wave, R wave and S wave. R wave is the most stable wave among them. In the physic field, R wave is defined as the first upward wave in QRS complex except for aVR lead in which QRS is inverted. Thus we detect it first. In *ECGDer*, the peak which has the maximal absolute derivative value *MADer* of QRS usually identifies one of the branches of R wave, as the Fig. 5 shows. If the peak value is positive, it locates the left branch and if it is negative, it locates the right branch.

An abnormal situation, as the Fig. 6 shows, is that when S wave is deep and large, and R wave is small due to the impact

Algorithm 1 Locating Reliable QRS Ranges

1: *condi*1_*flag* = **false**
2: *condi*2_*flag* = **false**
3: *intersection_number* = 0

4: **for** each $k \in [1, 12]$ **do**
5:    **if** ($k \neq i$) **and** (Intersect($qrs_{i,j}, qrs_k$) == **true**) **then**
6:       *intersection_number*++
7:    **end if**
8: **end for**

9: **if** *intersection_number* $\geq$ *min_intersection_number* **then**
10:    *condi*1_*flag* = **true**
11: **end if**

12: **if** ($qrs_{i,j} - qrs_{i,j-1}$) $\geq$ *min_distance* **then**
13:    *condi*2_*flag* = **true**
14: **end if**

15: **if** (*condi*1_*flag* == *true*) **and** (*condi*2_*flag* == *true*) **then**
16:    $qrs_{i,j}$ is accepted.
17: **else**
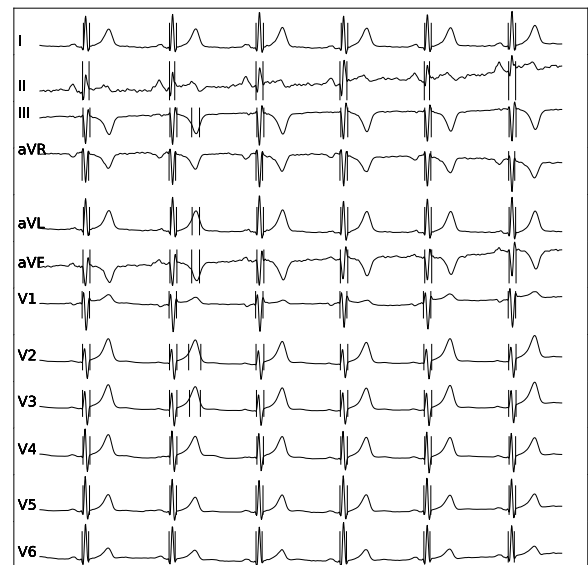18: $qrs_{i,j}$ is removed.
19: **end if**

FIGURE 4. An example of QRS detection in the LUDB database.

of heart disease, *MADer* might mark the right branch of S. If this case happens, using *MADer* to identify the location of R wave will mistakenly mark the right branch of S wave as the right branch of R wave. However, a fact is that though in this situation *MADer* marks the location of S, the left branch and right branch of R still has an absolute derivative value close to *MADer*. Taking these factors into account, we adopted a
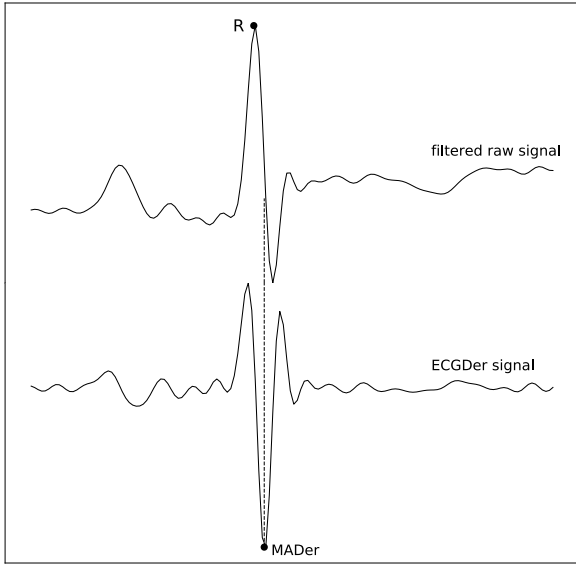
FIGURE 5. The filtered raw signal and its differentiated signal of a heat beat. *MADer* represents the peak where the absolute value is maximum.
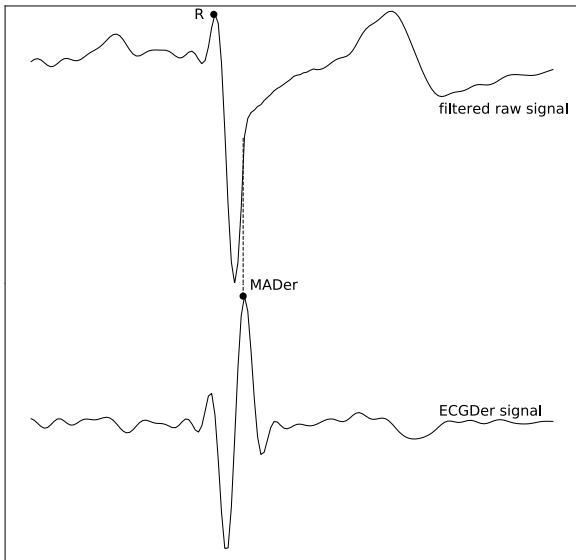

FIGURE 6. Deep and large S wave and small R wave. *MADer* represents the peak where the absolute value is maximum.
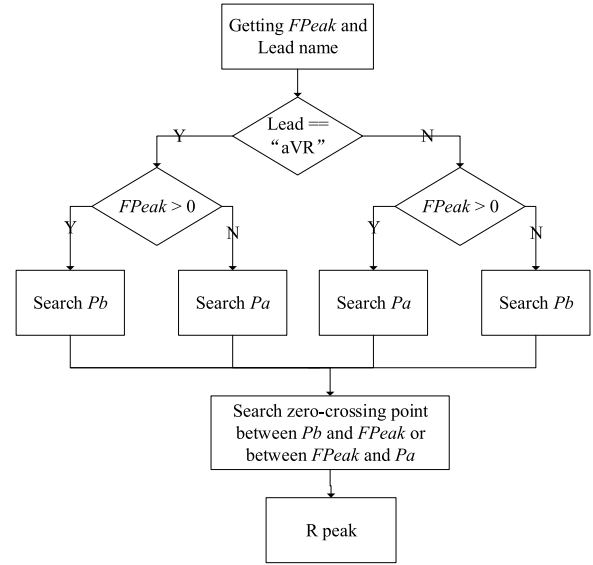

FIGURE 7. The flow chart of searching R peak.

In the following part of this section, *Pb* and *Pa* respectively denote the nearest peak before *FPeak* and the nearest peak after *FPeak* in *ECGDer* signal. Considering QRS is inverted in aVR and *FPeak* might recognize the right or left branch of R, we detect the position of R peak in four cases: first, if lead is aVR and the value of *FPeak* is greater than zero, we search zero-crossing point between *Pb* and *FPeak*; second, if lead is aVR and the value of *FPeak* is less than zero, we search zero-crossing point between *FPeak* and *Pa*; third, if lead is not aVR and the value of *FPeak* is greater than zero, we search zero-crossing point between *FPeak* and *Pa*; fourth, if lead is not aVR and the value of *FPeak* is less than zero, we search peak between *Pb* and *FPeak*. Finally, the location of the zero-crossing point in *ECGDer* signal is the location of R peak in raw signal. The whole process is described in the Fig. 7. In addition, to further ensure the correct recognition of R peaks, the locations of R peaks in the same beat in other leads were referred. Since the twelve-lead signals are recorded simultaneously, there should not be too much difference in the locations of the R peaks in the same beat. The most centralized peak locations were regarded as the correct locations. The selection process is described in detail in section II-D.2.

In QRS complex, Q wave is in front of R wave and S wave is behind R wave. Therefore, to detect the location of Q wave and S wave, we searched for the nearest peak forward and backward from the locations of R peaks in an interval of 80ms in the filtered signal. If not finding a peak in the time interval, we considered they are nonexistent.

C. P WAVE AND T WAVE LOCATION

The beat locations are determined by the mean value of R peak locations of the same beat in twelve-lead signals. Based on the beat locations, the wave signal window (P_{wave} and T_{wave}) and the adaptive search window (P_{search} and T_{search})

two-threshold technique to find the correct branch location of R wave as follows.

The two-threshold technique searches for the first peak *FPeak* forward in *ECGDer* where its absolute value is larger than a threshold H_{high}. If not finding, it uses a lower threshold H_{low} to search again. If found, *FPeak* is considered as identifying one of the branches of R. The formulas of the two thresholds are as follows. The larger the values of ε_1 and ε_2 is, the more likely the detected peak *FPeak* marks R wave. Thus, we set the values of ε_1 and ε_2 to 0.8 and 0.8 respectively.

$$H_{high} = \varepsilon_1 * MADer \qquad (4)$$

$$H_{low} = \varepsilon_2 * H_{high} \qquad (5)$$

are set for each P wave and T wave in each beat. Because the signal among wave window is used to decide the wave boundary and the signal among search window is used to decide the wave location, the range of wave window is larger than the range of search window.

When the distance between two beats is greater than 700ms, the corresponding P wave and T do not locate far from the QRS complex with the increase of the distance. So the range of wave window and the range of search window are determined by constant empirical values. When the distance between two beats is less than 700ms, it means that the distance between P wave and QRS complex and the distance between T wave and QRS complex will be flexible. So the range of wave window and the range of search window are determined by adaptive empirical values.

If b_n denotes the location at the n beat and RRT denotes the time interval between two neighbouring beats, the two window ranges of each wave are described as follows. It should be noted that P_{search} and T_{search} represent the offset range relative to b_n.

$$P_{wave} = \begin{cases} (b_n - 400ms, b_n) & RRT > 700ms \\ (b_n - 0.45 * RRT, b_n) & otherwise \end{cases} \quad (6)$$

$$P_{search} = \begin{cases} (-350ms, -80ms) & RRT > 700ms \\ (-0.5 * RRT, -60ms) & otherwise \end{cases} \quad (7)$$

$$T_{wave} = \begin{cases} (b_n, b_n + 550ms) & RRT > 700ms \\ (b_n, b_n + 0.75 * RRT) & otherwise \end{cases} \quad (8)$$

$$T_{search} = \begin{cases} (130ms, 490ms) & RRT > 700ms \\ (100ms, 0.7 * RRT) & otherwise \end{cases} \quad (9)$$

1) PREPROCESSING AND REJECTING ATRIAL FIBRILLATION

P wave and T wave have lower primary spectrum than QRS complex and are easily contaminated by high-frequency noise. We filtered them again by the low-pass Butterworth filter with a cutoff frequency of 20 Hz and four order to further smooth them.

When atrial fibrillation occurs, it makes no sense to recognize P wave and T wave. To refuse atrial fibrillation signal, the search window signals of P wave and T wave first were normalized to the zero-one range. It is understandable that when a wave exists a rising signal segment and a falling signal segment are bound to occur in the normalized signal and their amplitude ranges is enough large. Thus, the normalized signals were divided into a few monotone signal segments. Our algorithm then judged whether these signal segments satisfy the following two conditions: first, two contiguous signal segments—one is ascending and another is descending—exist; second, the range sizes of the amplitude of the two signal segments are greater than a threshold λ. If the normalized signal violated the two conditions, it was rejected. Tuning is the prevailing technique in machine learning which chooses a set of optimal hyperparameters for a learning algorithm. The value of λ is set to 0.4 after applying it.
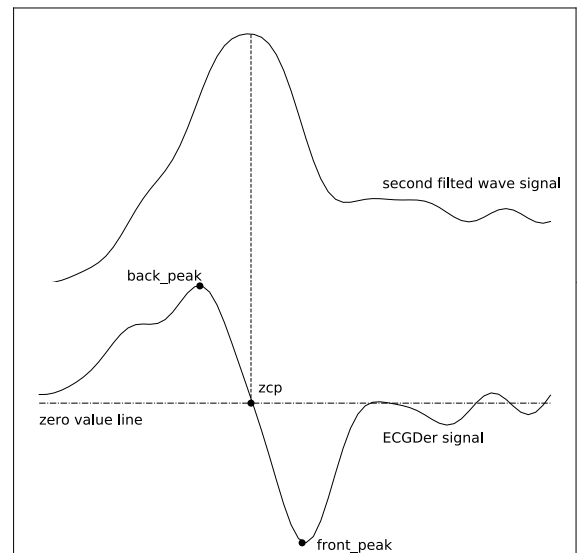

**FIGURE 8.** The location of P wave and T wave.

2) LOCATING WAVE

In the *ECGDer* signal of search window signal, the zero-crossing point was regarded as the location of the crucial wave. When noise is too loud, the number of the zero-crossing point may be more than one: one represents the crucial wave location and the rest represents the noise wave location. For different zero-crossing point, the nearest front peak and nearest back peak are different. In *ECGDer*, the zero-crossing point which represents the location of the crucial wave has the maximal sum of absolute value of nearest front peak and nearest back peak, as the Fig. 8 shows. Thus, we regarded such zero-crossing point as the correct wave location. Like the R wave, to further ensure correct recognition of the wave locations, among the twelve wave locations of the same beat for a given P wave or T wave, the most centralized wave locations were regarded as the correct locations. The selection process is described in detail in section II-D.2.

D. WAVE BOUNARY
1) SINGLE LEAD WAVEFORM BOUNDARY LOCATION

Local distance transform [32] refers to select an auxiliary segment containing the feature point extracted on the signal curve, then to calculate the distance between each point on the auxiliary segment and the segment line which is decided by linking the start and the end point of the auxiliary segment, and finally to identify the point of maximal distance as the signal curve feature point, namely the onset and the end of signal curve. It is acceptable to consider this point as the boundary of a wave as the point is the maximum curvature point. In this method, the quality of the auxiliary segment selection is directly related to the quality of the waveform boundary recognition. We deemed that an effective auxiliary segment should hold two conditions: first, at most one peak exists in the signal curve of auxiliary segment; second, the auxiliary segment should be long enough to hold the feature point needed.
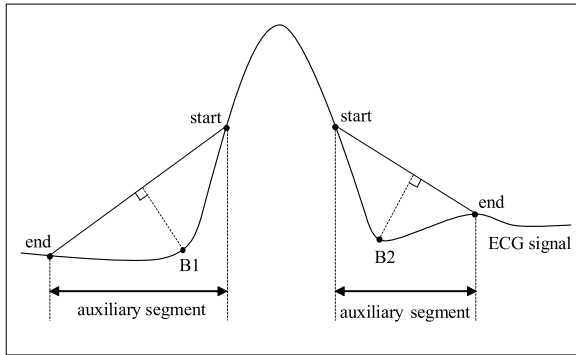
FIGURE 9. An example of using local distance transform to find the onset and end boundaries of a wave.

Fig. 9 shows an example of local distance transform for the onset and the end of a wave. Other wave boundaries, like QRS boundaries, are the same with this. For the onset of the wave, the auxiliary segment between the start point and the end point is effective because it not only contains the onset of the wave but also no more than one peak exists. The start point is the nearest derivative peak location to the wave peak location. And the end point is selected by the endpoint finding algorithm described in the later part of this subsection. We can see that B_1 is the farthest point on the auxiliary segment from the segment line. Visually, it is reasonable to regard it as the onset boundary of the wave. For the end of the wave, the signal curve of the auxiliary segment has a peak. Similarly, B_2 has also the farthest distance from the auxiliary segment line and is the reasonable end boundary of this wave. In this paper, different start points were chosen for different boundary types in different waves as follows.

- QRS onset: if Q wave exists, we search for the nearest peak backward from the location of Q wave in *ECGDer* signal and consider the peak location as the start point of the auxiliary segment in filtered signal; if Q wave is absent, we replace it with the location of R wave and do the same procedure.
- QRS end: if S wave exists, we search for the nearest peak forward from the location of S wave in *ECGDer* signal and consider its location as the start point of the auxiliary segment in filtered signal; if S wave is lost, we replace it with the location R wave and do the same procedure.
- T onset and end: we search for nearest peaks forward and backward respectively from the location of T wave in *ECGDer* signal and consider them as the start points of the auxiliary segment of onset and end in second-filtered wave signal.
- P onset and end: it is same with T wave.

A key idea to determine the endpoint of an effective auxiliary segment is to choose the next point to the endpoint of a monotonic interval which has the same monotony with *start* and it starts at *start* as the first candidate endpoint *c_end* and then assess whether the corresponding segment line intersects with the signal curve. If so, *c_end* should be updated to the nearest intersection point to *start*. Otherwise,

c_end recurrently is updated to the next point—for the onset wave, searching backward and for the end of wave, searching forward—and the new segment line is assessed until the distance between *c_end* and *start* is greater than the search limit. The final candidate endpoint *c_end* is the reasonable endpoint. The process is described in the Algorithm 2.

Algorithm 2 Finding Reasonable Endpoint of Auxiliary Segment

1: *c_end* = the next point to the endpoint of the monotonic interval.

2: *intersect_flag* = *Intersect*(*start*, *c_end*, *signal*) {The function of *Intersect* is to determine whether the line determined by *start* and *c_end* intersects with signal curve.}

3: **if** *intersect_flag* == **true then**
4:     *c_end* = the nearest intersection point to the *start* point.
5: **end if**

6: **while** the distance between *c_end* and *start* is less than the search limit **do**
7:     *intersect_flag* = *Intersect*(*start*, *c_end*, *signal*)
8:     **if** *intersect_flag* == **false then**
9:         *c_end* = the next point to the prior *c_end* point.
10:     **else**
11:         break
12:     **end if**
13: **end while**

14: the final *c_end* is the reasonable endpoint

In ECG, the duration of a normal P wave is less than 110ms; the duration of a normal QRS complex is among 60ms to 100ms; the duration of a normal T wave is between 100ms and 250ms. Taking these into account, we set different search limits of endpoints for different wave boundaries: for QRS complex boundary, when Q wave or S wave exist, the maximal time interval between *start* and *c_end* is 50ms, and when they are absent, the maximal time interval between *start* and *c_end* is 90ms; for P wave and T wave boundary, the maximal time interval between *start* and *c_end* is 100ms. After an effective auxiliary segment is chosen, the point on the auxiliary segment with the longest distance from the auxiliary segment line is recognized as the boundary point.

2) FINAL BOUNDARY DETERMINATION

Multiple annotations for the same type of wave boundary (p onset, p end, QRS onset, QRS end, T onset or T end) in a beat are obtained as each lead has its own annotation. To eliminate false wave boundaries, we select the most centralized annotations in a given window size as the correct annotation set. For the final onset of a type of
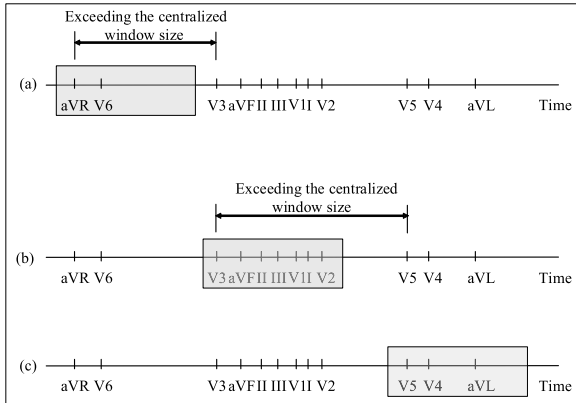
FIGURE 10. The final boundary determination rule for multi-leads.

FIGURE 11. The accuracy of feature points of crucial waves. The dark gray, black and light gray bars indicate the performance result of onset, peak and end of waves respectively.

wave in a beat, we choose the minimal annotation location value in the correct annotation set as the final onset. For the final end, reversely, we choose the maximal annotation location value.

Fig. 10 shows the decision process of final annotation of twelve-lead signals in a beat. We sort the twelve annotations in descending location order to determine the final onset and in ascending location order to determine the final end. Then a moving window divide the annotation array into several groups. As subplot (a) describes, the centralized window first includes the annotations of aVR and V6, because of the distance between the leftmost annotation, aVR, and the nearest unincluded annotation, V3, exceeding the window size. Then, it includes the annotations of V3, aVF, II, III, V1, I, V2, due to the distance between V3 and V5 exceeding the window size. The final group is V5, V4 and aVL.

We choose the group with the largest number of annotations as the correct group. In this figure, it is group 2. For onset, the annotation with the minimal location value in the correct group is the final onset of a beat, namely V3. For end, we choose the maximal time location, namely V2. To decide the final boundaries, we set the window size to 50ms for all kinds of wave boundaries. In section II-B.2 and section II-C, we detect the locations of R wave, P wave and T wave. To enhance the reliability of wave locations, we sort the multiple locations in a beat in ascending location order and also set the centralized window size to 50ms. The locations in the correct annotation set are then used to decide the waven boundaries in each lead.

III. RESULTS

We verified the availability of our algorithm on the LUDB database which records twelve-lead signals and has thorough annotations (including the peaks and boundaries of P waves in 1406 beats, QRS complexes in 1832 beats, and T waves in 1644 beat) of 200 individuals with various different heart diseases. The signal is digitized at 500 samples per second and the duration is 10 seconds. Considering twelve annotations exist for a type of wave boundary in a beat, for the purpose of the convenience of comparison, we calculated the
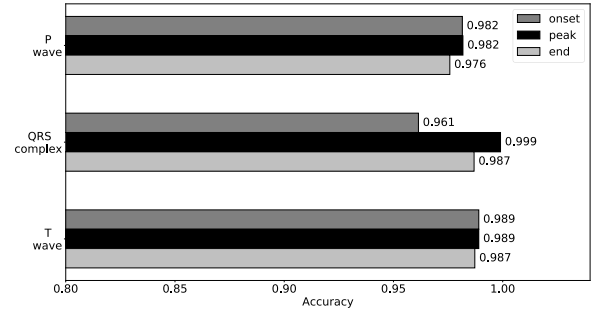
final boundary annotations for each detected beat of each record by the final boundary determination rule mentioned in section II-D.2. For the wave peak annotations (P peak, QRS complex peak and T peak), we chose the mean value of the multi detected wave peaks of the same wave type in a beat as the final peak annotations.

A. WAVE BOUNDARY AND PEAK PERFORMANCE EVALUATION

We set 40ms as a tolerance window interval for the correction detection of feature points since the accuracy of physicians analyzing ECG signal is 40ms. If the time difference between the algorithm annotation and its corresponding manual annotation is not beyond the tolerance, we deemed the algorithm annotation is correct. Otherwise, the algorithm annotation is wrong. Thus, the accuracy metrics can be formulated as $Accuracy = correct\_anns/total\_anns$ where $correct\_anns$ represents the correct annotations determined by the algorithm and $total\_anns$ represents the total annotations that has been marked manually in the database. Fig. 11 show the accuracy result of feature points of crucial waves.

From Fig. 11, our algorithm can reliably distinguish the peaks of P wave, T wave and especially QRS complex which can determine the R-R interval and thus indicate arrhythmia in the heart. The boundary accuracy of waves are also acceptable for physicians. Good detection of T wave end can help physicians determine whether Q-T interval changes, which is important for predicting malignant ventricular arrhythmia and sudden cardiac death.

B. ROBUSTNESS VERIFICATION FOR WAVE BOUNDARY DETERMINATION

To verify the Robustness of the method, in Fig. 12, we show the delineation performance for high T signal, high noise signal, and baseline drift signal in which the boundary determination of crucial waves is tough. In subplot (a), although the amplitudes of T waves are greater than QRS complexes, our algorithm can still distinguish them very well for the successful elimination of false QRS locations in section II-B.1. Subplot (b) is a noisy signal, but it has an insignificant impact on the correct identification of wave boundaries. In subplot (c), baseline drift noise affects the quality of the signal, which

TABLE 1. The comparison of delineation quality between our work and other algorithms in LUDB.Short horizontal lines denote missing metrics values.

		P onset	P peak	P end	QRS onset	QRS peak	QRS end	T onset	T peak	T end
Current work (*)	$Se(\%)$	98.43	98.43	98.43	99.89	100.00	99.89	99.21	99.27	99.21
	$PPV(\%)$	96.44	96.44	96.44	99.86	99.86	99.86	98.85	98.85	98.85
	$m \pm \sigma\,(ms)$	2.2±7.4	-0.76±5.5	-6.5±10.7	15.4±14.6	-0.14±3.4	-3.8±13.6	-1.3±8.8	-0.5±5.5	-1.2±6.8
Derivative threshold	$Se(\%)$	98.43	98.36	98.43	99.56	100.00	99.62	99.21	99.27	99.09
	$PPV(\%)$	96.44	96.44	96.44	99.86	99.86	99.86	98.85	98.85	98.85
	$m \pm \sigma\,(ms)$	2.8±7.5	-0.76±5.5	-7.3±10.1	18.4±14.7	-0.14±3.4	-5.4±14.3	-2.6±11.4	-0.5±5.5	-3.3±7.3
Kalyakulina *et al.* [33]	$Se(\%)$	98.46	98.46	98.46	99.61	–	99.61	–	99.03	98.03
	$PPV(\%)$	96.41	96.41	96.41	99.87	–	99.87	–	98.84	98.84
	$m \pm \sigma\,(ms)$	-2.7±10.2	-0.3±6.2	0.4±11.4	-8.1±7.7	–	3.8±8.8	–	4.0±7.4	5.7±15.5
$2\sigma CSE\,(ms)$		10.2	–	12.7	6.5	–	11.6	–	–	30.6

(a)

(b)

(c)
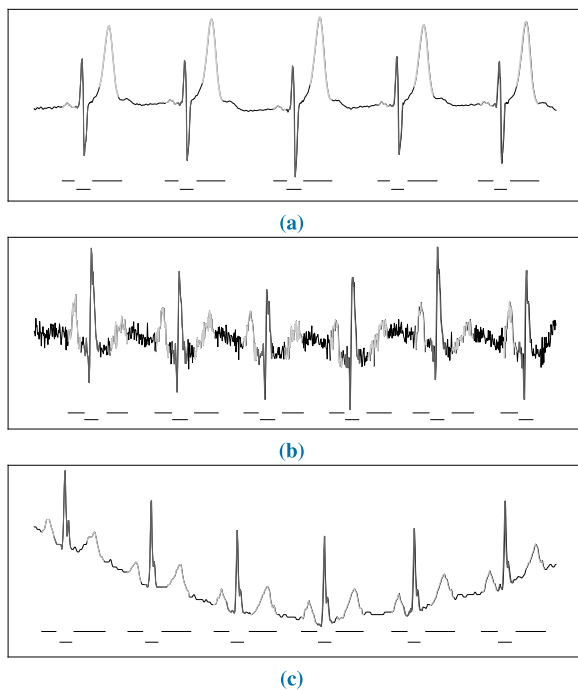
FIGURE 12. Three cases where wave boundaries are difficult to determine. (a) High T wave occurs; (b) High noise exists; (c) Baseline drift appears. The horizontal line below signal curve in each subgraph represents the waveform area manually labeled. In the signal curve, a good detection result—QRS complex (dark gray signal curve), P and T wave (pale gray signal curve)—can be observed.

makes it difficult to decide the boundaries of ECG waves by the method of derivative threshold. However, our algorithm can also handle it.

C. PERFORMANCE COMPARISON WITH OTHER WORKS

Kalyakulina *et al.* [33] proposed a delineation algorithm based on wavelet transform and evaluated its performance with a tolerance window interval of 150ms. If a feature point is detected correctly, the result is counted as true positive *TP* and the mismatch between automated and manual annotation is calculated as an error. If only automated annotation exists,

a false positive result *FP* is counted. Reversely, when only manual annotation exists, a false negative *FN* result occurs. The authors identified the quality of the algorithm by four metrics: average error *m*, standard deviation σ, sensitivity $Se\,(\%) = TP/(TP + FN)$ and positive predictive value $PPV\,(\%) = TP/(TP + FP)$. We adopted the same metrics to compare our work with it.

In addition, a classical method to determine the waveform boundary is to use the derivative threshold [2]–[4]. This method determines a suitable wave boundary by judging whether the wave signal curve intersects with a derivative threshold. If so, the corresponding intersection point is considered as the appropriate wave boundary. But in this method, how to choose a suitable derivative threshold is a intractable problem. Traditionally, the derivative threshold can be adaptively determined by dividing the derivative extremum on the left and right sides of the wave by a given constant value. To compare our method with it, we keep the other experimental conditions unchanged and only use the derivative threshold method to determine the boundary. When Q wave or S wave does not exist, we divide the derivative extremum of the left and right branch of R wave by a given constant value to determine the boundary of QRS complex. We set this constant value to 6. When Q wave and S wave exist, we use them to determine the boundary of QRS complex and set this value to 4. The boundary of P wave and T wave is determined in the same way and the constant value is also 4.

It should be noted that we calculate the error by the minimal difference between the final annotation and its corresponding twelve manual annotations in a beat for a given wave annotation type. The comparison result is shown in Table 1. The experimental data for wavelet-based method are derived from the work of Kalyakulina *et al.* [32].

We can find that the feature point recognition of P wave, QRS complex, and T wave has a sensitivity value greater than 98% and has a positive predictive value greater than 96%. The standard values for P wave boundary and T wave end do not exceed the limits set by CSE party [34] and the standard value of QRS end is close to its limit. In addition, our algorithm

has a better performance than derivative threshold method and does not need to set parameters when determining the boundaries of crucial waves. At the same time, our algorithm almost has the same performance as the wavelet-based algorithm when decide the locations of crucial waves and a better result when determine the onset of P wave and the end of T wave. These indicate the availability of our method.

IV. CONCLUSION

In this paper, an algorithm for delineating P wave, QRS complex, and T wave is developed by utilizing twelve-lead signals. QRS detector identifies the locations of QRS complexes in each lead, and then false QRS locations are removed by taking other leads into account. Based on this, the range of wave search window is decided to detect the location of P wave and T wave. In each lead, the local distance transform method finds the reasonable boundaries of the crucial waves. Considering that the annotations of a specific boundary types in one lead should not differ significantly from the same annotations in other leads, a final boundary decision rule is applied to reject the erroneous annotations caused by noise. Its performance has been verified with the LUDB database.

The results suggest that the peak accuracies of P wave, QRS complex and T wave all are above 98%, and the boundary accuracy of these waves is also above 96%. Our algorithm also is tested on several particular situations where the boundary recognition of crucial waves are tough such as high T wave, high noisy signal and baseline wandering. The results prove that our algorithm can handle these situations very well. In comparing with other works, our method does not need to set thresholds when determining the boundaries of crucial waves as the derivative threshold method does, which reduces the parameters of the algorithm and eliminates the selection of wavelet basis to determine wave boundaries as the wavelet-based method does, but it can still achieve the performance similar to those methods.

Accordingly, it was concluded that the developed algorithm has a desirable capability in delineating the peaks and boundaries of the crucial wave. The result can further be utilized to get the morphological information and time interval information of crucial waves which will improve the performance of the automatic diagnosis system of cardiovascular diseases.

REFERENCES

[1] F. A. Elhaj, N. Salim, A. R. Harris, T. T. Swee, and T. Ahmed, "Arrhythmia recognition and classification using combined linear and nonlinear features of ECG signals," *Comput. Methods Programs Biomed.*, vol. 127, pp. 52–63, Apr. 2016.

[2] J. Pan and W. J. Tompkins, "A real-time QRS detection algorithm," *IEEE Trans. Biomed. Eng.*, vol. BME-32, no. 3, pp. 230–236, Mar. 1985.

[3] P. Laguna, N. V. Thakor, P. Caminal, R. Jané, H.-R. Yoon, A. B. De Luna, V. Marti, and J. Guindo, "New algorithm for QT interval analysis in 24-hour holter ECG: Performance and applications," *Med. Biol. Eng. Comput.*, vol. 28, no. 1, pp. 67–73, Jan. 1990.

[4] P. Laguna, R. Jané, and P. Caminal, "Automatic detection of wave boundaries in multilead ECG signals: Validation with the CSE database," *Comput. Biomed. Res.*, vol. 27, no. 1, pp. 45–60, Feb. 1994.

[5] C. Li, C. Zheng, and C. Tai, "Detection of ECG characteristic points using wavelet transforms," *IEEE Trans. Biomed. Eng.*, vol. 42, no. 1, pp. 21–28, Jan. 1995.

[6] J. Martinez, R. Almeida, S. Olmos, A. Rocha, and P. Laguna, "A wavelet-based ECG delineator: Evaluation on standard databases," *IEEE Trans. Biomed. Eng.*, vol. 51, no. 4, pp. 570–581, Apr. 2004.

[7] A. Ghaffari, M. Homaeinezhad, M. Akraminia, M. Atarod, and M. Daevaeiha, "A robust wavelet-based multi-lead electrocardiogram delineation algorithm," *Med. Eng. Phys.*, vol. 31, no. 10, pp. 1219–1227, Dec. 2009.

[8] M. Yochum, C. Renaud, and S. Jacquir, "Automatic detection of P, QRS and T patterns in 12 leads ECG signal based on CWT," *Biomed. Signal Process. Control*, vol. 25, pp. 46–52, Mar. 2016.

[9] V. Afonso, W. Tompkins, T. Nguyen, and S. Luo, "ECG beat detection using filter banks," *IEEE Trans. Biomed. Eng.*, vol. 46, no. 2, pp. 192–202, 1999.

[10] Y. Sun, K. L. Chan, and S. M. Krishnan, "Characteristic wave detection in ECG signal using morphological transform," *BMC Cardiovascular Disorders*, vol. 5, p. 28, Sep. 2005.

[11] R. Andreao, B. Dorizzi, and J. Boudy, "ECG signal analysis through hidden Markov models," *IEEE Trans. Biomed. Eng.*, vol. 53, no. 8, pp. 1541–1549, Aug. 2006.

[12] A. Zifan, S. Saberi, M. H. Moradi, and F. Towhidkhah, "Automated ECG segmentation using piecewise derivative dynamic time warping," *Int. J. Biol. Med. Sci.*, vol. 1, no. 3, pp. 181–285, 2006.

[13] I. Saini, D. Singh, and A. Khosla, "P- and T-wave delineation in ECG signals using support vector machine," *IETE J. Res.*, vol. 59, no. 5, p. 615, 2013.

[14] S. Mehta and N. Lingayat, "Application of support vector machine for the detection of P- and T-waves in 12-lead electrocardiogram," *Comput. Methods Programs Biomed.*, vol. 93, no. 1, pp. 46–60, Jan. 2009.

[15] I. Saini, D. Singh, and A. Khosla, "K-nearest neighbour-based algorithm for P- and T-waves detection and delineation," *J. Med. Eng. Technol.*, vol. 38, no. 3, pp. 115–124, Apr. 2014.

[16] S. Pal and M. Mitra, "Empirical mode decomposition based ECG enhancement and QRS detection," *Comput. Biol. Med.*, vol. 42, no. 1, pp. 83–92, Jan. 2012.

[17] S. Sahoo, T. Das, and S. Sabut, "Adaptive thresholding based EMD for delineation of QRS complex in ECG signal analysis," in *Proc. Int. Conf. Wireless Commun., Signal Process. Netw. (WiSPNET)*, Mar. 2016.

[18] D. Rezgui and Z. Lachiri, "Detection of ECG beat using ensemble empirical mode decomposition," in *Proc. 7th Int. Conf. Modelling, Identificat. Control (ICMIC)*, Dec. 2015.

[19] X. Ning and I. W. Selesnick, "ECG enhancement and QRS detection based on sparse derivatives," *Biomed. Signal Process. Control*, vol. 8, no. 6, pp. 713–723, Nov. 2013.

[20] N. Bayasi, T. Tekeste, H. Saleh, A. Khandoker, B. Mohammad, and M. Ismail, "Adaptive technique for P and T wave delineation in electrocardiogram signals," in *Proc. 36th Annu. Int. Conf. IEEE Eng. Med. Biol. Soc.*, Aug. 2014.

[21] C. Lin, G. Kail, A. Giremus, C. Mailhes, J.-Y. Tourneret, and F. Hlawatsch, "Sequential beat-to-beat P and T wave delineation and waveform estimation in ECG signals: Block Gibbs sampler and marginalized particle filter," *Signal Process.*, vol. 104, pp. 174–187, Nov. 2014.

[22] M. Rakshit, D. Panigrahy, and P. K. Sahu, "EKF with PSO technique for delineation of P and T wave in electrocardiogram(ECG) signal," in *Proc. 2nd Int. Conf. Signal Process. Integr. Netw. (SPIN)*, Feb. 2015.

[23] B. S. Shaik, G. V. S. S. K. R. Naganjaneyulu, and A. Narasimhadhan, "A novel approach for QRS delineation in ECG signal based on chirplet transform," in *Proc. IEEE Int. Conf. Electron., Comput. Commun. Technol. (CONECCT)*, Jul. 2015.

[24] T. Dózsa and P. Kovács, "ECG signal compression using adaptive hermite functions," in *Proc. Int. Conf. ICT Innov.*, vol. 399, 2016, pp. 245–254.

[25] S. Lee, Y. Jeong, D. Park, B.-J. Yun, and K. Park, "Efficient fiducial point detection of ECG QRS complex based on polygonal approximation," *Sensors*, vol. 18, no. 12, p. 4502, Dec. 2018.

[26] G. Moody and R. Mark, "The impact of the MIT-BIH arrhythmia database," *IEEE Eng. Med. Biol. Mag.*, vol. 20, no. 3, pp. 45–50, May 2001.

[27] A. Taddei, G. Distante, M. Emdin, P. Pisani, G. B. Moody, C. Zeelenberg, and C. Marchesi, "The European ST-T database: Standard for evaluating systems for the analysis of ST-T changes in ambulatory electrocardiography," *Eur. Heart J.*, vol. 13, no. 9, pp. 1164–1172, Sep. 1992.

[28] P. Laguna, R. G. Mark, A. Goldberg, and G. B. Moody, "A database for evaluation of algorithms for measurement of QT and other waveform intervals in the ECG," in *Proc. Comput. Cardiol.*, Sep. 1997, pp. 673–676.

[29] J. L. Willems, "Common standards for quantitative electrocardiography," *J. Med. Eng. Technol.*, vol. 9, no. 5, p. 209, 1985.

[30] A. I. Kalyakulina, I. I. Yusipov, and V. A. Moskalenko, "Lu electrocardiography database: A new open-access validation tool for delineation algorithms," 2018, *arXiv:1809.03393v2*. [Online]. Available: https://arxiv.org/abs/1809.03393v2

[31] C. Xi-Wu and D. Qin-Kai, "Frequency analysis on the ECG waveform," *Chin. J. Med. Phys.*, vol. 18, no. 1, pp. 46–48, 2001.

[32] L. Mao, "P wave detection in ECG signal based on location estimation and recognition post-processing," *Signal Process.*, vol. 25, no. 6, pp. 948–952, 2009.

[33] A. I. Kalyakulina, I. I. Yusipov, V. A. Moskalenko, A. V. Nikolskiy, A. A. Kozlov, N. Y. Zolotykh, and M. V. Ivanchenko, "Finding morphology points of electrocardiographic-signal waves using wavelet analysis," *Radiophys. Quantum Electron.*, vol. 61, nos. 8–9, pp. 689–703, Jan. 2019.

[34] N. Listed, "Recommendations for measurement standards in quantitative electrocardiography. the cse working party," *Eur. Heart J.*, vol. 6, no. 10, pp. 815–825, 1985.

JIAJIAN ZHANG received the B.E. degree in software engineering from Shandong University, in 2017. He is currently pursuing the master's degree in computer techniques with Zhejiang University. His current research interests include machine learning, medical image analysis, and GPU acceleration.

GENLANG CHEN received the Ph.D. degree in computer science from Zhejiang University, China, in 2012. He was a Researcher of computer engineering with the University of Arkansas, from January 2014 to January 2015. He is currently an Associate Professor with the Ningbo Institute of Technology, Zhejiang University. His current research areas are in the data mining, machine learning and big data application, which include deep learning and parallel computing, data mining and big data application for healthcare, multiscale modeling of complex networks, and programming models on hybrid computer networks.

LIANG ZHANG received the bachelor's degree in computer science from Ningbo University, China, in 2005. He has been working with the Ningbo Center for Disease Control and Prevention, since July 2005. He is currently the Deputy Director of the Ningbo Big Data Research Institute of Public Health, and mainly involved in regional public health informatization construction, information security management, and the research on big data of health.

MAOLIN CHEN received the B.E. degree in software engineering from the Chengdu University of Information Technology, in 2017. He is currently pursuing the master's degree in computer techniques with Zhejiang University. His current research interests include machine learning, medical signal analysis, and pattern recognition.

CHAOYI PANG is currently a Senior Member of ACM. He received the Ph.D. degree from the University of Melbourne, in 1999. He worked in IT industrial as an IT Engineer and a Consultant, from 1999 to 2002, and CSIRO as a Research Scientist, Australia, from 2002 to 2014. He is currently the Dean of the School of Computer and Data Engineering, Zhejiang University. His research interests include algorithm, stream data compression and processing, data warehousing, data integration, database theory, graph theory, and e-health.

● ● ●